# Charge Transfer and Orbital Reconstruction at an Organic−Oxide Interface

Marco Caputo, Michał Studniarek, Eduardo Bonini Guedes, Luca Schio, Kassymkhan Baiseitov, Niéli Daffé, Nicolas Bachellier, Alla Chikina, Giovanni Di Santo, Alberto Verdini, Andrea Goldoni, Matthias Muntwiler, Cinthia Piamonteze, Luca Floreano, Milan Radovic,* and Jan Dreiser*

ABSTRACT: The two-dimensional electron system (2DES) located at the surface of strontium titanate (STO) and at several other STO-based interfaces has been an established platform for the study of novel physical phenomena since its discovery. Here we report how the interfacing of STO and tetracyanoquinodimethane (TCNQ) results in a charge transfer that depletes the number of free carriers at the STO surface, with a strong impact on its electronic structure. Our study paves the way for efficient tuning of the electronic properties, which promises novel applications in the framework of oxide/organic-based electronics.
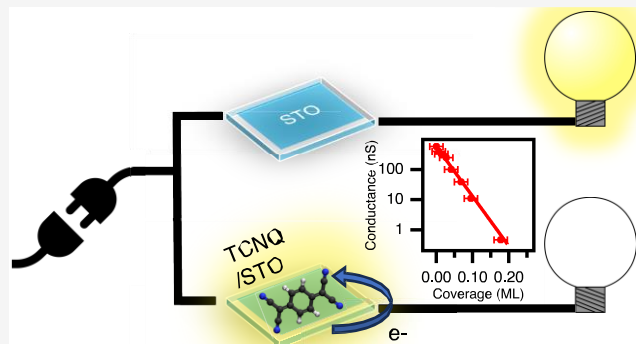
SrTiO3 (STO) is a perovskite-type transition metal oxide, intensely studied due to its unique properties such as superconductivity[1] and ferroelectricity.[2−4] The robustness and intriguing properties of a high-mobility electron gas at the interface between STO and LaAlO3 (LAO),[5] among others, has further fueled the research on various STO-based heterostructures.[6−8] Similarly, at the surface of STO, a two- dimensional electron system (2DES) can be formed by irradiation with ultraviolet light[9] or in situ cleaving.[10] To this end, it is of ultimate interest to explore different strategies to tune the 2DES properties, tailoring them for various needs. A promising strategy is to add suitable adsorbates on the STO surface, exploiting the surface nature of the 2DES. Oxygen- deficient STO thin films show high conductivity variation in response to the oxygen[11,12] or ethanol[13] concentration of the gas they are in contact with. Similarly, hydrogen adsorption on the surface is reported to have a surface doping effect, with a metallic state appearing at the Fermi level[14] equivalent to n-doping.[15] In an analogous way, it has been shown that the protonation state of the LAO surface has a dramatic impact on the conductivity at the LAO/STO interface.[16,17] In order to achieve less volatile devices, molecular building blocks commonly used in organic electronics and spintronic heterostructures are advantageous. The resulting organic− oxide interfaces exhibit huge variability arising from the vast number of combinations of the two constituents. They allow to exploit the chemical functionalization[18] and the multifunction-

ality of molecules,[19] which were proven useful in spin valves[20] and photoswitchable logic.[21]

In this work, we investigate the effect of the adsorption of the organic electron acceptor tetracyanoquinodimethane (TCNQ) on the electronic properties of the vacuum-annealed STO surface. We show through *in situ* electrical transport and synchrotron-based near-edge X-ray absorption fine structure (NEXAFS) measurements that the molecular adsorption results in a charge transfer from the STO surface to the TCNQ layer. This is followed by a reorganization of the Ti 3d orbitals at the STO surface, as proven by X-ray absorption spectroscopy (XAS) as well as by resonant and nonresonant photoemission spectroscopy (ResPES and PES).

Figure 1a displays the $I(V)$ characteristics obtained for the vacuum-annealed (500 °C, 30 min—hereinafter denoted as pristine) STO and for different coverages of TCNQ, which was sublimed from a Knudsen cell, on STO. All samples exhibit ohmic $I(V)$ behavior as manifested in the linear $I(V)$; however, upon deposition of TCNQ, the conductance drops dramatically. Note that the conductance of the pristine sample may
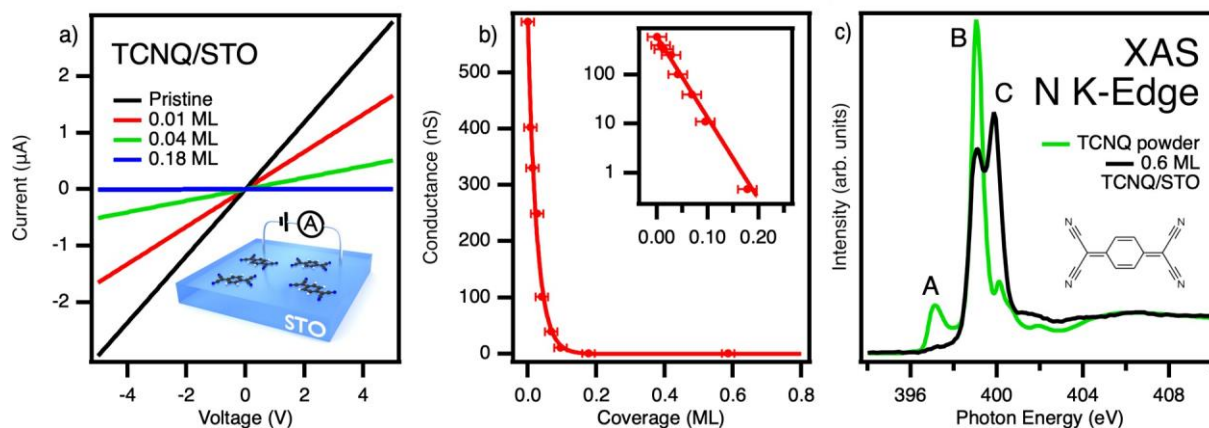
Figure 1. Electrical properties of the TCNQ/STO interface and adsorption behavior of TCNQ. (a) $I(V)$ characteristics of STO(100) as a function of TCNQ coverage. (b) Evolution of conductance as a function of molecular coverage in units of molecular monolayers (MLs). Symbols and the solid line denote experimental data and the best-fit curve, respectively, as explained in the text. The inset contains the same data in a semilogarithmic scale. Measurements were performed in ultrahigh vacuum at room temperature. (c) Nitrogen K-edge NEXAFS obtained on a TCNQ powder sample (green curve) and on a 0.6 ML TCNQ/STO interface (the latter one obtained at the magic angle; see the Methods section). In the inset, a ball-and-stick representation of the TCNQ molecule with the central benzene backbone and the four cyano groups on the sides is shown.
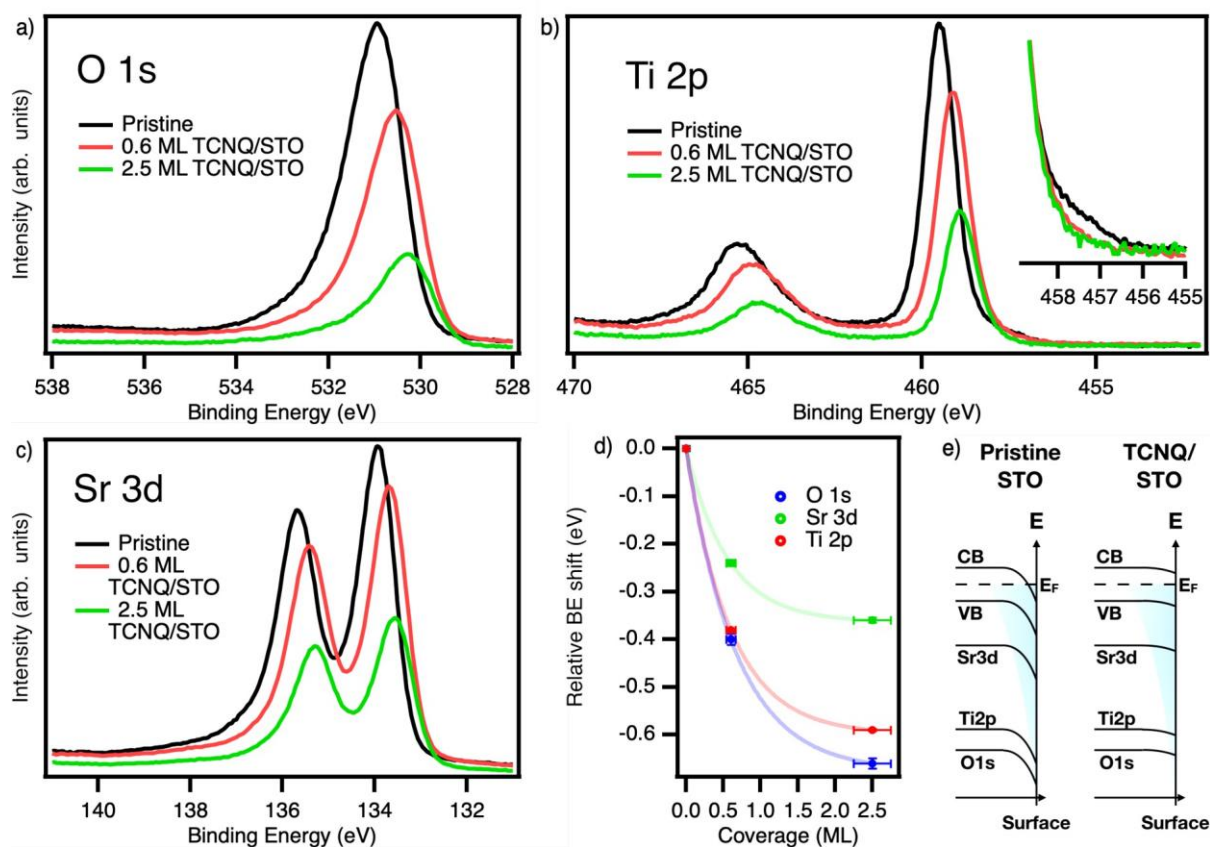

Figure 2. Coverage-dependent PES reveals lowering of binding energy and band flattening: (a) O 1s peak, (b) Ti 2p peak, and (c) Sr 3d peak. In the inset of panel b, the region of the Ti^{3+} peak: in this case, all peaks have been aligned and normalized to the pristine one. All spectra have been acquired at room temperature and at a photon energy of $h\nu = 650$ eV.

(d) Relative binding energy shift as a function of TCNQ coverage; lines are guides for the eye. (e) Scheme of the band bending (not to scale) occurring at the surface of bare annealed STO (left) and TCNQ/STO (right). The cyan shadowed region is the one photoemission is sensitive to.

include a contribution from the contact resistance of the bond wires. However, for TCNQ coverages larger than a few percent of the STO surface, the effect of the contact resistance, which is independent of the TCNQ coverage, becomes negligible.

The corresponding coverage-dependent conductance values extracted from the $I(V)$ measurements are plotted in Figure 1b, revealing that the electrical conductance drops by more than 3 orders of magnitude from 600 nS of the pristine STO
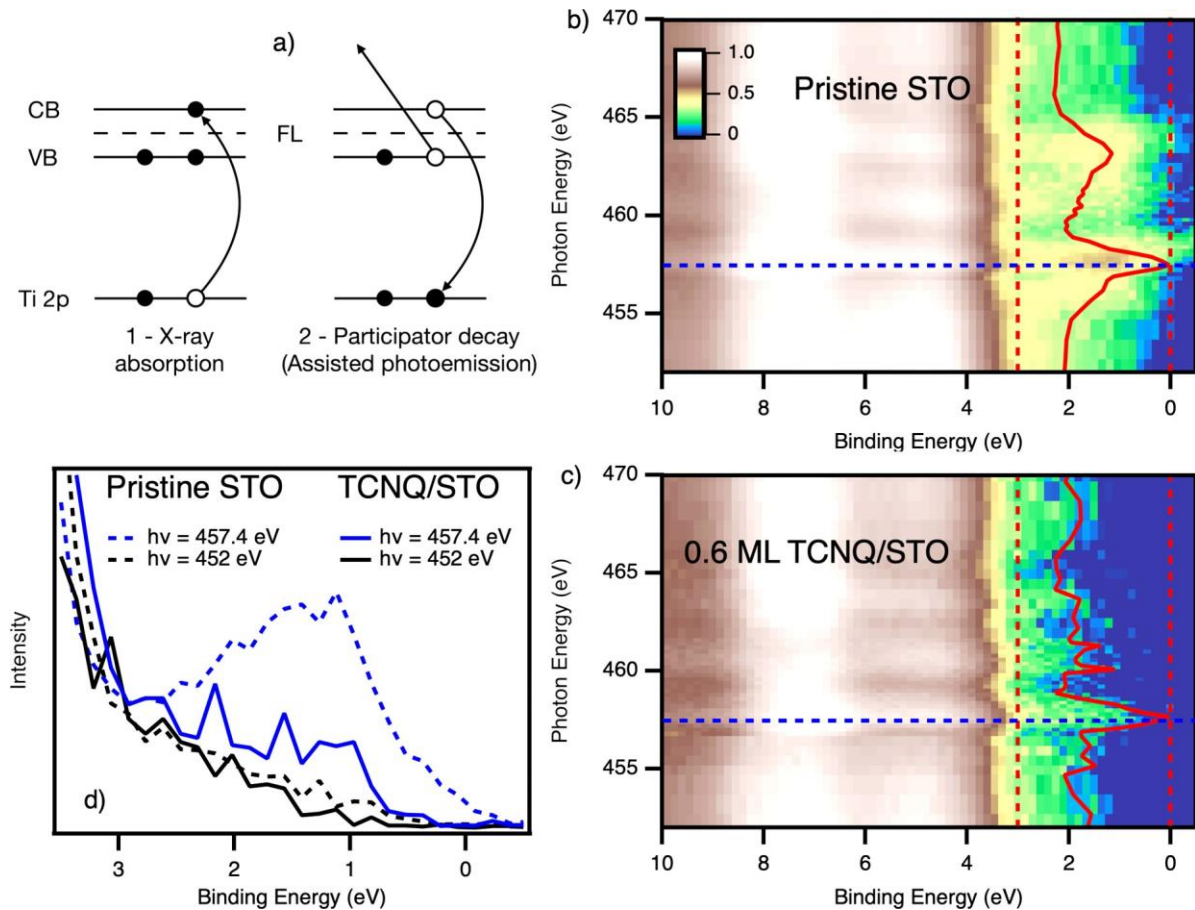
Figure 3. Resonant photoemission. (a) Schematic of the core hole-assisted photoemission process. (b, c) Valence band intensity maps across the Ti $L_{2,3}$-edges for pristine STO and 0.6 ML TCNQ/STO interface, respectively (color code in the inset): the red curves denote the CIS integrated over the in-gap states (exact regions marked with dashed lines of the same color). (d) Single valence band spectra acquired at notable photon energies: $hv = 452$ eV (off-resonance) in black; $hv = 457.4$ eV (strongest resonance in both CISs) in blue.

down to 0.5 nS upon deposition of only 0.18 monolayers (MLs) of TCNQ. Here, a ML is defined as a densely packed layer of molecules in flat adsorption geometry. A sub-ML denotes a partial molecular coverage with molecules with uncovered portions. Figure 1b reveals that at low coverages the conductance σ depends exponentially on the TCNQ coverage x (in units of MLs) $\sigma(x) = \sigma_0 e^{R_0 x}$, where σ_0 is the conductance of the annealed STO before deposition and R_0 contains the coverage dependence. Fitting yields a remarkably large value of $R_0 = 38 \pm 4.3$ ML^{-1} reflecting the enormous coverage dependence of the surface conductance and $\sigma_0 =$ 590.1 $\pm$ 0.1 nS. Note that the strong dependence on the molecular coverage confirms that the observed change in conductance occurs at the TCNQ/STO interface. Two factors may lead to the reduction of the conductance at the STO surface: (i) the reduction of the charge carrier mobility or (ii) the reduction of the number of charge carriers contributing to the electrical

transport. Below, we will demonstrate that the second mechanism is the main driving force, owing to a charge transfer from the surface of STO to the electron-accepting molecules, with the effect of depleting the number of carriers responsible for the surface conductivity.

The NEXAFS at the nitrogen K-edge displayed in Figure 1c supports this hypothesis: the TCNQ powder spectrum shows three main resonances at photon energies of (A) 397.4, (B) 399.1, and (C) 399.9 eV. Peak A corresponds to the π^* lowest

unoccupied molecular orbital (LUMO), mostly localized on the benzene backbone, while peaks B and C originate from σ^* and π^* symmetry molecular orbitals localized on the cyano groups.[22] Molecules adsorbed on the STO surface, however, hardly display any trace of the LUMO resonance: its quenching is characteristic of negatively charged $TCNQ^{-1}$ molecules having an aromatic central ring,[22−25] confirming the electron transfer to the molecules from the substrate.

A charge transfer across the interface must have an influence also on the 2DES and on the electronic structure of the surface of STO. Figure 2a−c displays coverage-dependent PES, showing the evolution of the photoemission peaks of the substrate. All of them exhibit an attenuation of the total intensity and a peak shift toward a lower binding energy upon increasing TCNQ coverage.

The intensity decrease is due to the inelastic scattering of photoelectrons crossing the molecular overlayer, and its magnitude is kinetic energy dependent: the higher the electron kinetic energy (hence, the lower the binding energy), the less pronounced this effect is. The same tendency is also observed for the binding energy shift: the higher the binding energy, the more pronounced the shift, as is visible in Figure 2d. This similarity suggests that the binding energy shift is depth- dependent, which is consistent with a lowering of the band bending that is present on the pristine STO surface, as illustrated in Figure 2e.
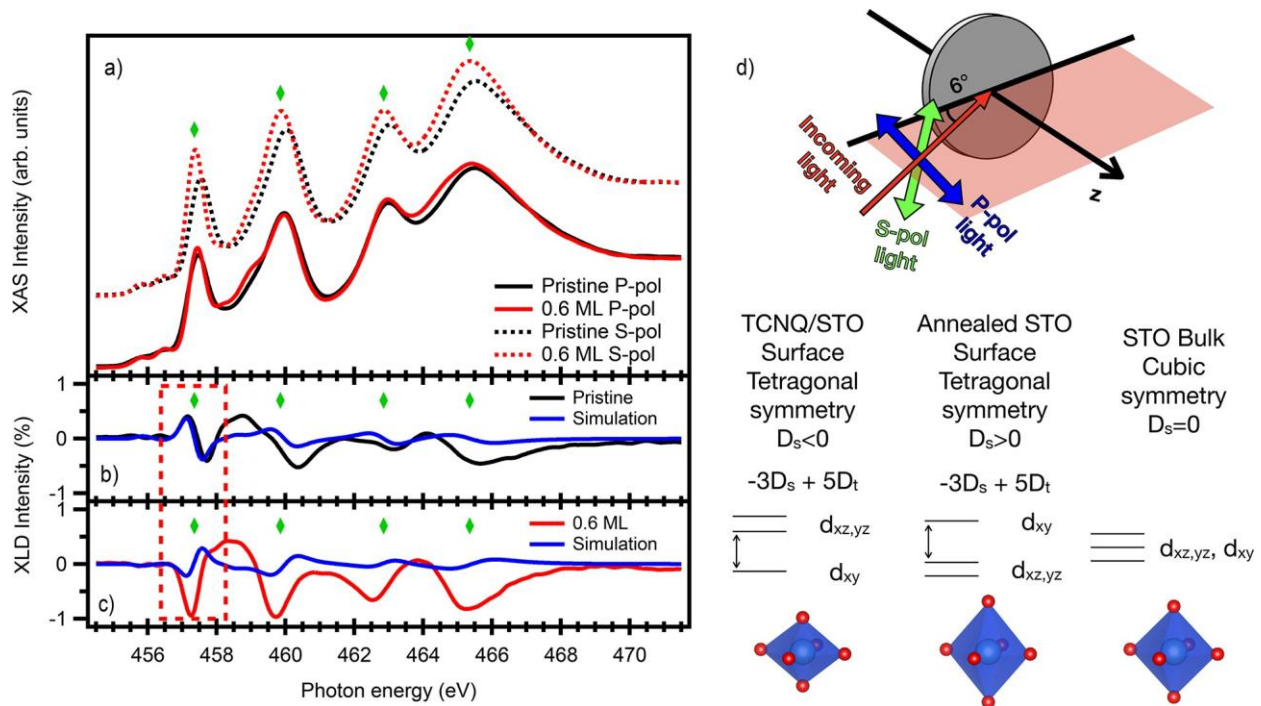
Figure 4. X-ray linear dichroism at the Ti $L_{2,3}$s-edges. (a) XAS acquired in partial electron yield with s-polarized (solid lines) and p-polarized light (dashed lines) for the pristine (black lines) and TCNQ-deposited (red lines) samples. Panels b and c show the corresponding XLD spectra. The blue lines represent calculated XLD spectra with $D_s < 0$ and $D_s > 0$ respectively, for the TCNQ/STO and pristine STO samples. Panel d sketches the experimental geometry (top) and the different crystal distortions giving rise to the calculated spectra.

Bulk STO is a wide band gap ($\Delta_{gap} = 3.2$ eV) semiconductor[26] with the Fermi level close to the conduction band (CB) minimum.[14,27–29] While in bulk stoichiometric STO no surface state was found, resulting in negligibly small band bending at the surface,[30] annealing in UHV at 300 °C for several hours results in a conducting surface.[31] This accumulation of negative charges at the surface, together with the downward band bending,[32] corresponds to the case of surface n-doping as shown in Figure 2e. Upon TCNQ adsorption, the charge transfer across the interface depletes the 2DES, with the effect of flattening the bands, as illustrated in Figure 2e. In the case of the deep core levels such as O 1s and Ti 2p the photoelectrons originate from the very surface of STO, where the effect of band movement upon charge depletion is strongest. On the other hand, the photoelectrons coming from the Sr 3d core level travel not only from the surface but also from a slightly deeper region in bulk (as highlighted by the cyan region in Figure 2e), where the effect of surface band bending is weaker.

Photoemission results also yield specific information about the oxidation state of the Ti ions in STO. The inset of Figure 2b shows the low binding energy region of the Ti $2p_{3/2}$ peak. Here, all peaks in the graph were aligned with those of the pristine sample and normalized to the same height. The pristine spectrum obtained on pristine STO shows a shoulder at $E_B = 457.3$ eV, which is commonly associated with the presence of Ti^{3+} species in STO. Like in the case of reduced TiO_2, the presence of the Ti^{3+} shoulder is always accompanied by the appearance of in-gap states due to the partial filling of the Ti 3d unoccupied states.[33–36] The Ti^{3+} shoulder disappears completely upon TCNQ deposition, at both coverages of 0.6 and 2.5 MLs, indicating a surface containing only Ti^{4+} species. Tracking the corresponding behavior of the in-gap states upon

TCNQ deposition, however, is not straightforward because of the possible overlap of the TCNQ highest occupied molecular orbital (HOMO) and filled LUMO states in this energy region.[37]

In order to disentangle the in-gap states at the STO surface from the contributions of the molecular orbitals, we used core−hole assisted resonant photoemission, i.e., measure the valence band photoemission at incoming photon energies resonant with the Ti L_3-edge. In this case, predominantly the spectral features associated with states having contributions from Ti 3d orbitals are excited and thus enhanced,[38] due to the very short range of the mechanism of excitation decay (Auger process).[39] Figure 3a shows the schematics of this process: a photon resonant with the core level → conduction band transition excites the system, which then decays following (among the others) the depicted participator decay, whose final state is equivalent to the one of the direct photoemission, but with several orders of magnitude higher cross section. In Figure 3b,c we report the valence band photoemission spectra on pristine STO and 0.6 ML of TCNQ/STO as a function of the incoming photon energy. The intensity variation of the binding energy region integrated in the range 0−3 eV is overplotted as a red line in the 2D color maps. This profile, called constant initial state (CIS), gives information on the response to different excitation energies of the photoemission yield of specific states, in this case, the region containing the in- gap states. In both cases of pristine STO and 0.6 ML TCNQ/ STO, the CIS shows a resonance at E_{phot} = 457.4 eV, corresponding to the Ti $2p_{3/2}$ → 3d t_{2g} transition. The strong CIS resonance at the blue dotted line and the tail

extending up to the Fermi level highlight the presence of the in-gap states. Figure 3d displays horizontal cuts of the maps along the blue dotted lines in Figure 3b,c in the range of E_B =

0−3 eV at the photon energies indicated in the plot. In both cases, the photoemission intensity in the in-gap region is enhanced across the resonance: the area under the spectrum in the region 0−3 eV of binding energy increases by a factor of
3.4 at E_{phot} = 457.4 eV with respect to the off-resonance
spectrum. In the case of the 0.6 ML TCNQ/STO, however, the in-gap region shows negligible intensity enhancement: the blue spectrum shows an increase of the area in the region 0−3 eV of a factor of 1.6, that is, less than half with respect to the pristine STO case (47%).

Taking into account only the attenuation of the photo- emission intensity due to the TCNQ molecules using Lambert−Beer's law, an intensity drop to 85% would be expected. Therefore, the observed drop to 47% implies that the photoemission intensity is strongly reduced upon TCNQ adsorption. This spectral weight reduction points to a depopulation of the in-gap states due to an electron transfer from the substrate into the TCNQ molecular orbitals, like formerly demonstrated for the quenching of the $TiO_2(110)$ defect state by adsorption of perylene tetracarboxylic diimide[38] as well as for C_{60}/TiO_x.[40]

Finally, it is worth taking into consideration the surface stoichiometry of the STO surface. Although it has been shown that even a moderate thermal treatment can result in the presence of different surface terminations,[41] this does not have an influence on the results and conclusions drawn in the present work. Moreover, TCNQ itself does not contain oxygen atoms; therefore, the disappearance of the Ti^{3+} peak and in-gap states cannot be related to any filling of oxygen vacancies, and it must be ascribed exclusively to the transfer of charges occurring across the interface.

Like photoemission, Ti L-edge XAS and X-ray linear dichroism (XLD) are excellent tools to compare the electronic structure changes between the TCNQ/STO interface and the pristine STO. Figure 4a shows the XAS acquired in S and P polarizations of 0.6 ML of TCNQ/STO and of pristine STO, with the corresponding XLD spectra shown in panels b and c. Upon molecular adsorption, the XLD signal in the region between 456.5 and 458.5 eV (corresponding to the Ti $2p_{3/2} \rightarrow 3d\ t_{2g}$ transition—highlighted by a red box in the figure) is reversed, as already observed in STO upon LAO coverage.[42] Multiplet calculations shown in panels b and c can qualitatively describe this behavior by breaking the cubic symmetry of the bulk and reversing the sign of D_s from +20 meV in the annealed case[43,44] to −20 meV after deposition of TCNQ. The D_s parameter in the calculations corresponds to the energy splitting between the in-plane and out-of-plane orbitals in the t_{2g} manifold, and its change of sign indicates an orbital reorganization at the STO surface upon molecular adsorption. In the pristine sample, the $d_{xz/yz}$ orbitals are lowest in energy, while after deposition, the d_{xy} orbital becomes the

lowest, as highlighted in Figure 4d. More details can be found in the Supporting Information. The orbital reorganization may be due to molecule−substrate hybridization and the subsequent modification of the effective crystal field[15] and/or structural distortions at the STO surface that have been shown to have a profound impact on the properties of the 2DES at the surface of STO.[45]

In conclusion, we have combined *in situ* electronic transport,
X-ray absorption spectroscopy, and (resonant) photoemission to study the impact of the adsorption of TCNQ on the electronic properties and the surface conductance of $SrTiO_3(100)$. The adsorption of a submonolayer amount of

TCNQ on STO leads to a massive suppression of the electrical conductance at the STO surface by several orders of magnitude. Nitrogen K-edge absorption spectra reveal that this effect arises from a charge transfer from the substrate toward the molecules, while core-level photoemission evidenced that this charge transfer reduces the band bending at the surface. Also, upon charge transfer Ti^{3+} ions at the STO surface are converted into Ti^{4+} ones, and the in-gap states of STO are depleted. X-ray absorption spectroscopy reveals a change from elongatedtoward compressed oxygen octahedra surrounding the Ti ions upon TCNQ adsorption, which implies a reordering of the Ti 3d orbitals.

We emphasize that these effects are stable at room temperature because of the nonvolatility of the organic molecules used. One way to create nanodevices could be by the controlled, local deposition of organic molecules to write features onto the oxide surface, which would allow for a dramatic improvement of the minimum feature size compared to state-of-the-art lithography techniques. We demonstrate a new class of hybrid organic−oxide materials appealing for devices, sensors, and energy-related applications. The versatility, chemical tunability, and multifunctionality of oxide and molecular materials give rise to an impressive potential for future applications. These include the use of molecular units with different electron-accepting or -donating properties and the exploitation of other multifunctional building blocks such as photoactive units exhibiting intramolecular charge transfer.

METHODS

Substrate Preparation. The TiO_2-terminated undoped STO(100) (SurfaceNet GmbH, Germany) of dimensions 4.8
$\times$ 5 mm^2, thickness 0.5 mm, one-side polished, was wedge bonded prior to the experiment and introduced into ultrahigh vacuum ($p \sim 10^{-10}$ mbar). The separation between the leads at the STO surface was 4.5 ± 0.2 mm. STO was annealed at 773 K for 30 min to remove contamination and to prepare atomically flat terraces.[46] The annealed STO surface was checked by low energy electron diffraction (LEED), exhibiting the expected 1×1 pattern (see Figure S2).[31] A similar but Nb- doped substrate was prepared in an analogous manner with
and without TCNQ and checked by scanning tunneling microscopy (Supporting Information). The sample preparation and the electrical transport measurements were performed within the same ultrahigh-vacuum environment of the X- Treme beamline at the Swiss Light Source, Paul Scherrer Institut,[47] in the absence of X-rays.

Molecule Deposition. TCNQ was sublimed in ultrahigh vacuum ($p \sim 10^{-10}$ mbar) from a Knudsen cell held at 368 K resulting in low deposition rates (0.04−0.1 monolayers/min) onto the substrate held at room temperature. The deposition rates were determined by using a quartz crystal microbalance.

Electrical Transport Measurements. The conductance of the STO surface was measured using two wedge-bonded contacts in ultrahigh vacuum and at room temperature. The two-point measurement, as opposed to more sophisticated (e.g., van der Pauw like) schemes, is sufficient here because of the significant initial and further increasing (upon molecule deposition) resistance of the STO surface, rendering the resistance of the wires and contacts negligible. The conductance was calculated from the slope of the $I(V)$ characteristics acquired using a Keithley 6517B sourcemeter. The error bars are within the symbol size.

X-ray Spectroscopy. XAS at the Ti L-edges and the N K- edge were performed at room temperature in partial electron yield mode (PEY) at the ALOISA beamline at Elettra.[48] A manipulator collinear with horizontally polarized synchrotron light rotates around its axis to change the geometry from s- to p-polarization while the angle of incidence of light is fixed to 6°. The XLD was calculated as $\mu^P - \mu^S$, where μ^i denotes the corresponding absorption spectra for the two linear polar- izations.

Photoemission Spectroscopy. All measurements were performed at room temperature at the ALOISA beamline at Elettra[48] using 0.5 wt % Nb:STO as substrate. Electrons were collected using a hemispherical analyzer at normal emission, while the angle of incidence of light was kept at 4°. 0.6 ML TCNQ/STO did not show any sign of degradation under the beam, while 2.5 ML TCNQ/STO showed a slow degradation, which was mediated by illuminating different spots on the surface.

Ligand-Field Multiplet Calculations. The Ti L2,3 XAS were simulated using multiplet calculations, including ligand field effects, using the CTM4XAS interface.[49,50] Details and best-fit parameters are given in the caption of Figure S1.

Supporting Information

Ligand-field multiplet calculations, low-energy electron diffraction data, and scanning tunneling microscopy data

AUTHOR INFORMATION
Corresponding Authors

Milan Radovic − *Swiss Light Source, Paul Scherrer Institut, 5232 Villigen PSI, Switzerland*; Email: milan.radovic@ psi.ch

Jan Dreiser − *Swiss Light Source, Paul Scherrer Institut, 5232 Villigen PSI, Switzerland;* ⓞ orcid.org/0000-0001-7480- 1271; Email: jan.dreiser@psi.ch

Authors

Marco Caputo − *Elettra Sincrotrone Trieste, 34149 Trieste, Italy; MAX IV Laboratory, Lund University, 22100 Lund, Sweden;* ⓞ orcid.org/0000-0001-7452-0998

Michał Studniarek − *Swiss Light Source, Paul Scherrer Institut, 5232 Villigen PSI, Switzerland*

Eduardo Bonini Guedes − *Swiss Light Source, Paul Scherrer Institut, 5232 Villigen PSI, Switzerland*

Luca Schio − *Laboratorio TASC, Istituto Officina dei Materiali (IOM)-CNR, 34149 Trieste, Italy*

Kassymkhan Baiseitov − *Swiss Light Source, Paul Scherrer Institut, 5232 Villigen PSI, Switzerland*

Niéli Daffé − *Swiss Light Source, Paul Scherrer Institut, 5232 Villigen PSI, Switzerland;* ⓞ orcid.org/0000-0002-2225- 1658

Nicolas Bachellier − *Swiss Light Source, Paul Scherrer Institut, 5232 Villigen PSI, Switzerland*

Alla Chikina − *Swiss Light Source, Paul Scherrer Institut, 5232 Villigen PSI, Switzerland*

Giovanni Di Santo − *Elettra Sincrotrone Trieste, 34149 Trieste, Italy;* ⓞ orcid.org/0000-0001- 9394-2563

Alberto Verdini − *Laboratorio TASC, Istituto Officina dei Materiali (IOM)-CNR, 34149 Trieste, Italy;* ⊙ orcid.org/ 0000-0001-8880-2080

Andrea Goldoni − *Elettra Sincrotrone Trieste, 34149 Trieste, Italy*

Matthias Muntwiler − *Swiss Light Source, Paul Scherrer Institut, 5232 Villigen PSI, Switzerland;* ⊙ orcid.org/0000- 0002-6628-3977

Cinthia Piamonteze − *Swiss Light Source, Paul Scherrer Institut, 5232 Villigen PSI, Switzerland;* ⊙ orcid.org/0000- 0002-8416-9668

Luca Floreano − *Laboratorio TASC, Istituto Officina dei Materiali (IOM)-CNR, 34149 Trieste, Italy;* ⊙ orcid.org/ 0000-0002-3654-3408

Complete contact information is available at:
https://pubs.acs.org/10.1021/acs.nanolett.3c03713

Author Contributions

M.C. and M.S. contributed equally to this work.

Notes

The authors declare no competing financial interest.

REFERENCES

(1) Schooley, J. F.; Hosler, W. R.; Cohen, M. L. Superconductivity in semiconducting $SrTiO_3$. *Phys. Rev. Lett.* 1964, *12*, 474−475.

(2) Bickel, N.; Schmidt, G.; Heinz, K.; Müller, K. Ferroelectric relaxation of the $SrTiO_3(100)$ surface. *Phys. Rev. Lett.* 1989, *62*, 2009−2011.

(3) Haeni, J. H.; et al. Room-temperature ferroelectricity in strained $SrTiO_3$. *Nature* 2004, *430*, 758−761.

(4) Jang, H. W.; et al. Ferroelectricity in strain-free $SrTiO_3$ thin films. *Phys. Rev. Lett.* 2010, *104*, 197601.

(5) Ohtomo, A.; Hwang, H. Y. A high-mobility electron gas at the $LaAlO_3/SrTiO_3$ heterointerface. *Nature* 2004, *427*, 423−426.

(6) Cen, C.; Thiel, S.; Hammerl, G.; Schneider, C. W.; Andersen, K. E.; Hellberg, C. S.; Mannhart, J.; Levy, J. Nanoscale control of an interfacial metal−insulator transition at room temperature. *Nat. Mater.* 2008, *7*, 298−302.

(7) Mannhart, J.; Schlom, D. G. Oxide interfaces—an opportunity for electronics. *Science* 2010, *327*, 1607−1611.

(8) Pai, Y.-Y.; Tylan-Tyler, A.; Irvin, P.; Levy, J. Physics of $SrTiO_3$-based heterostructures and nanostructures: a review. *Rep. Prog. Phys.* 2018, *81*, 036503.

(9) Meevasana, W.; King, P. D. C.; He, R. H.; Mo, S.-K.; Hashimoto, M.; Tamai, A.; Songsiriritthigul, P.; Baumberger, F.; Shen, Z.-X. Creation and control of a two-dimensional electron liquid at the bare $SrTiO_3$ surface. *Nat. Mater.* 2011, *10*, 114−118.

(10) Santander-Syro, A. F.; et al. Two-dimensional electron gas with universal subbands at the surface of $SrTiO_3$. *Nature* 2011, *469*, 189− 193.

(11) Meixner, H.; Gerblinger, J.; Lampe, U.; Fleischer, M. Thin-film gas sensors based on semiconducting metal oxides. *Sens. Actuators, B* 1995, *23*, 119−125.

(12) Bando, H.; Aiura, Y.; Haruyama, Y.; Shimizu, T.; Nishihara, Y. Structure and electronic states on reduced $SrTiO_3$(110) surface observed by scanning tunneling microscopy and spectroscopy. *J. Vac. Sci. Technol., B: Microelectron. Nanometer Struct.−Process., Meas., Phenom.* 1995, *13*, 1150−1154.

(13) Hodak, S. K.; Supasai, T.; Wisitsoraat, A.; Hodak, J. H. Design of low cost gas sensor based on $SrTiO_3$ and $BaTiO_3$ films. *J. Nanosci. Nanotechnol.* 2010, *10*, 7236−7238.

(14) D'Angelo, M.; Yukawa, R.; Ozawa, K.; Yamamoto, S.; Hirahara, T.; Hasegawa, S.; Silly, M. G.; Sirotti, F.; Matsuda, I. Hydrogen- Induced Surface Metallization of $SrTiO_3$(001). *Phys. Rev. Lett.* 2012, *108*, 116802.

(15) Lin, F.; Wang, S.; Zheng, F.; Zhou, G.; Wu, J.; Gu, B.-L.; Duan, W. Hydrogen-induced metallicity of $SrTiO_3$ (001) surfaces: A density functional theory study. *Phys. Rev. B* 2009, *79*, 035311.

(16) Scheiderer, P.; Pfaff, F.; Gabel, J.; Kamp, M.; Sing, M.; Claessen, R. Surface-interface coupling in an oxide heterostructure: Impact of adsorbates on $LaAlO_3$/$SrTiO_3$. *Phys. Rev. B* 2015, *92*, 195422.

(17) Brown, K. A.; He, S.; Eichelsdoerfer, D. J.; Huang, M.; Levy, I.; Lee, H.; Ryu, S.; Irvin, P.; Mendez-Arroyo, J.; Eom, C.-B.; Mirkin, C. A.; Levy, J. Giant conductivity switching of $LaAlO_3$/$SrTiO_3$ heterointerfaces governed by surface protonation. *Nat. Commun.* 2016, *7*, 10681.

(18) Kumar, K. S.; Studniarek, M.; Heinrich, B.; Arabski, J.; Schmerber, G.; Bowen, M.; Boukari, S.; Beaurepaire, E.; Dreiser, J.; Ruben, M. Engineering On-Surface Spin Crossover: Spin-State Switching in a Self-Assembled Film of Vacuum-Sublimable Functional Molecule. *Adv. Mater.* 2018, *30*, 1705416.

(19) Coronado, E. Molecular magnetism: from chemical design to spin control in molecules, materials and devices. *Nat. Rev. Mater.* 2020, *5*, 87−104.

(20) Dediu, V. A.; Hueso, L. E.; Bergenti, I.; Taliani, C. Spin routes in organic semiconductors. *Nat. Mater.* 2009, *8*, 707−716.

(21) Andréasson, J.; Pischel, U.; Straight, S. D.; Moore, T. A.; Moore, A. L.; Gust, D. All-Photonic Multifunctional Molecular Logic Device. *J. Am. Chem. Soc.* 2011, *133*, 11641−11648.

(22) Fraxedas, J.; Lee, Y.; Jiménez, I.; Gago, R.; Nieminen, R. M.; Ordejón, P.; Canadell, E. Characterization of the unoccupied and partially occupied states of TTF-TCNQ by XANES and first- principles calculations. *Phys. Rev. B* 2003, *68*, 195115.

(23) Tseng, T.-C.; Urban, C.; Wang, Y.; Otero, R.; Tait, S. L.; Alcamí, M.; Écija, D.; Trelka, M.; Gallego, J. M.; Lin, N.; et al. Charge-transfer-induced structural rearrangements at both sides of organic/metal interfaces. *Nat. Chem.* 2010, *2*, 374−379.

(25) Bässler, M.; Fink, R.; Buchberger, C.; Väterlein, P.; Jung, M.; Umbach, E. Near edge X-ray absorption fine structure resonances of quinoide molecules. *Langmuir* 2000, *16*, 6674−6681.

(26) Sing, M.; Meyer, J.; Hoinkis, M.; Glawion, S.; Blaha, P.; Gavrila, G.; Jacobsen, C. S.; Claessen, R. Structural vs electronic origin of renormalized band widths in TTF-TCNQ: An angular dependent NEXAFS study. *Phys. Rev. B* 2007, *76*, 245119.

(27) Adeagbo, W. A.; Fischer, G.; Hergert, W. First-principles investigations of electronic and magnetic properties of $SrTiO_3$(001) surfaces with adsorbed ethanol and acetone molecules. *Phys. Rev. B* 2011, *83*, 195428.

(28) Aiura, Y.; Nishihara, Y.; Haruyama, Y.; Komeda, T.; Kodaira, S.; Sakisaka, Y.; Maruyama, T.; Kato, H. Effects of surface oxygen vacancies on electronic states of TiO_2(110), TiO_2(001) and $SrTiO_3$(001) surfaces. *Phys. B* 1994, *194*, 1215−1216.

(29) Haruyama, Y.; Aiura, Y.; Bando, H.; Suzuki, H.; Nishihara, Y. Surface electronic structure of electron-doped $SrTiO_3$. *Phys. B* 1997, *237*, 380−382.

(30) Cardona, M. Optical Properties and Band Structure of $SrTiO_3$ and $BaTiO_3$. *Phys. Rev.* 1965, *140*, A651.

(31) Adachi, Y.; Kohiki, S.; Wagatsuma, K.; Oku, M. Intrinsic and extrinsic surface states of single crystalline SrTiO₃. *J. Appl. Phys.* 1998, *84*, 2123−2126.

(32) Di Capua, R.; Radovic, M.; De Luca, G. M.; Maggio-Aprile, I.; Miletto Granozio, F.; Plumb, N. C.; Ristic, Z.; Scotti di Uccio, U.; Vaglio, R.; Salluzzo, M. Observation of a two-dimensional electron gas at the surface of annealed SrTiO₃ single crystals by scanning tunneling spectroscopy. *Phys. Rev. B* 2012, *86*, 155425.

(33) Zhang, Z.; Yates, J. T., Jr. Band bending in semiconductors: chemical and physical consequences at surfaces and interfaces. *Chem. Rev.* 2012, *112*, 5520−5551.

(34) Hong, H.; McChesney, J. L.; Wrobel, F.; Yan, X.; Li, Y.; Bhattacharya, A.; Fong, D. D. In situ study on the evolution of atomic and electronic structure of LaTiO₃/SrTiO₃ system. *Phys. Rev. Mater.* 2022, *6*, L011401.

(35) Plumb, N. C.; et al. Mixed Dimensionality of Confined Conducting Electrons in the Surface Region of SrTiO₃. *Phys. Rev. Lett.* 2014, *113*, 086801.

(36) Strocov, V. N.; Chikina, A.; Caputo, M.; Husanu, M.-A.; Bisti, F.; Bracher, D.; Schmitt, T.; Miletto Granozio, F.; Vaz, C. A. F.; Lechermann, F. Electronic phase separation at LaAlO₃/SrTiO₃ interfaces tunable by oxygen deficiency. *Phys. Rev. Mater.* 2019, *3*, 106001.

(37) Walker, S. M.; Bruno, F. Y.; Wang, Z.; de la Torre, A.; Riccó, S.; Tamai, A.; Kim, T. K.; Hoesch, M.; Shi, M.; Bahramy, M. S.; King, P. D. C.; Baumberger, F. Carrier-Density Control of the SrTiO₃ (001) Surface 2D Electron Gas studied by ARPES. *Adv. Mater.* 2015, *27*, 3894−3899.

(38) Capitán, M. J.; Álvarez, J.; Navio, C. Study of the electronic structure of electron accepting cyano-films: TCNQ versus TCNE. *Phys. Chem. Chem. Phys.* 2018, *20*, 10450−10459.

(39) Lanzilotto, V.; Lovat, G.; Fratesi, G.; Bavdek, G.; Brivio, G. P.; Floreano, L. TiO₂(110) charge donation to an extended π-conjugated molecule. *J. Phys. Chem. Lett.* 2015, *6*, 308−313.

(40) Verdini, A.; Krüger, P.; Floreano, L. In *Surface Science Techniques*; Bracco, G., Holst, B., Eds.; Springer: Berlin, 2013; pp 217−247.

(41) Amelot, D.; Ahmadpour, M.; Ros, Q.; Cruguel, H.; Casaretto, N.; Cossaro, A.; Floreano, L.; Madsen, M.; Witkowski, N. Decipher- ing Electron Interplay at the Fullerene/Sputtered TiOx Interface: A Barrier-Free Electron Extraction for Organic Solar Cells. *ACS Appl. Mater. Interfaces* 2021, *13*, 19460−19466.

(41) Sokolović, I.; Franceschi, G.; Wang, Z.; Xu, J.; Pavelec, J. c. v.; Riva, M.; Schmid, M.; Diebold, U.; Setvín, M. Quest for a pristine unreconstructed SrTiO₃(001) surface: An atomically resolved study via noncontact atomic force microscopy. *Phys. Rev. B* 2021, *103*, L241406.

(42) Salluzzo, M.; Gariglio, S.; Torrelles, X.; Ristic, Z.; Di Capua, R.; Drnec, J.; Sala, M. M.; Ghiringhelli, G.; Felici, R.; Brookes, N. B. Structural and electronic reconstructions at the LaAlO₃/SrTiO₃ interface. *Adv. Mater.* 2013, *25*, 2333−2338.

(43) Maurel, L.; Herrero-Martin, J.; Motti, F.; Vasili, H. B.; Piamonteze, C.; Heyderman, L. J.; Scagnoli, V. Route to tunable room temperature electric polarization in SrTiO₃ − CoFe₂O₄ hetero- structures. *J. Mater. Chem. C* 2021, *9*, 5977−5984.

(44) Di Capua, R.; et al. Orbital selective switching of ferromagnetism in an oxide quasi two-dimensional electron gas. *npj Quantum Materials* 2022, *7*, 41.

(45) Guedes, E. B.; Muff, S.; Brito, W. H.; Caputo, M.; Li, H.; Plumb, N. C.; Dil, J. H.; Radović, M. Universal Structural Influence on the 2D Electron Gas at SrTiO₃ Surfaces. *Adv. Sci.* 2021, *8*, 2100602.

(46) Nishimura, T.; Ikeda, A.; Namba, H.; Morishita, T.; Kido, Y. Structure change of TiO₂-terminated SrTiO₃(001) surfaces by annealing in O₂ atmosphere and ultrahigh vacuum. *Surf. Sci.* 1999, *421*, 273−278.

(47) Piamonteze, C.; Flechsig, U.; Rusponi, S.; Dreiser, J.; Heidler, J.; Schmidt, M.; Wetter, R.; Calvi, M.; Schmidt, T.; Pruchova, H.; Krempasky, J.; Quitmann, C.; Brune, H.; Nolting, F. X-Treme

beamline at SLS: X-ray magnetic circular and linear dichroism at high field and low temperature. *J. Synchrotron Radiat.* 2012, *19*, 661−674.

(48) Floreano, L.; Naletto, G.; Cvetko, D.; Gotter, R.; Malvezzi, M.; Marassi, L.; Morgante, A.; Santaniello, A.; Verdini, A.; Tommasini, F.; et al. Performance of the grating-crystal monochromator of the ALOISA beamline at the Elettra Synchrotron. *Rev. Sci. Instrum.* 1999, *70*, 3855−3864.

(49) Stavitski, E.; de Groot, F. M. The CTM4XAS program for EELS and XAS spectral shape analysis of transition metal L-edges. *Micron* 2010, *41*, 687−694.

(50) Cowan, R. D. *The Theory of Atomic Structure and Spectra; Los Alamos Series in Basic and Applied Sciences*; University of California Press, Ltd.: Berkeley, CA, 1981.